Characterizing the Fluorescence Intermittency and Photobleaching Kinetics of Dye Molecules Immobilized on a Glass Surface

Edwin K. L. Yeow,* Sergey M. Melnikov, Toby D. M. Bell, Frans C. De Schryver, and Johan Hofkens*

Department of Chemistry, Katholieke Universiteit Leuven, Celestijnenlaan 200F, B-3001 Heverlee, Belgium

Received: September 27, 2005; In Final Form: November 29, 2005

The blinking behavior of single Atto565 molecules on a glass surface is studied under air or nitrogen atmospheres using confocal microscopy. The broad distributions for both on- and off-time durations obey power law kinetics that are rationalized using a charge tunneling model. In this case, a charge is transferred from the Atto565 molecule to localized states found on the glass surface. Subsequent charge recombination by back charge tunneling from trap to Atto565 cation (i.e., dark state) restores the fluorescence. The off-time distribution is independent of excitation intensity (*I*), whereas the on-time distribution exhibits a power law exponent that varies with *I*. Two pathways have been identified to lead to the formation of the radical dark state. The first involves direct charge tunneling from the excited singlet S_1 state to charge traps in the surrounding matrix, and the second requires charge ejection from the triplet T_1 state after intersystem crossing from S_1. Monte Carlo simulation studies complement the two-pathway model. Photobleaching curves of both single and ensemble molecules do not exhibit monoexponential decays suggesting complex bleaching dynamics arising from triplet and radical states.

1. Introduction

Photoblinking and photobleaching are important characteristics of single molecules. Photoblinking refers to the temporary disappearance of emitted light when molecules undergo reversible transitions between "on" and "off" states, whereas photobleaching is an irreversible process where bleached products that do not absorb or emit at the excitation and emission wavelengths, respectively, are formed from the molecule. In many applications of single molecule spectroscopy there is a pertinent need to increase the photostability of fluorescent probes and to avoid interruptions during light emission which may otherwise interfere with the actual processes under investigation (e.g., protein folding,[1] enzyme catalysis,[2] electron transfer[3]).

To increase the efficacy of fluorescent probes, it is important to first understand the dynamics behind photobleaching and photoblinking. Even though many studies have been dedicated to unraveling the mechanisms responsible for these two processes, there still remain controversies surrounding the nature of the dark states, and the pathways leading to their formation.[4−11]

Fluorescence intermittency of single molecules has previously been explained in terms of triplet state dynamics,[12,13] molecular reorientation,[11] spectral diffusion,[15] conformational changes,[8,9] and intramolecular electron transfer.[3,14] More recently, on/off events following power law distributions for an ensemble of single molecules have been reported. Haase et al. observed long-lived dark states that obey power law distributions for perylenemonoimide chromophores embedded in poly(methyl methacrylate) film,[16] and Schuster et al. reported similar power law blinking behavior for various dye molecules (e.g., rhodamine 6G, terrylene) dispersed on top of glass surfaces and polymer films.[17,18] Hoogenboom et al. reported a power law distributed dark state for a trimer molecule consisting of three rigidly linked tetraphenoxyperylene diimide chromophores.[19] A model based on the formation of (dark) radical cations arising from electron transfer between chromophores and self-trapped states found in the host matrix has been used to understand the sensitivity of power law kinetics to environmental polarity. The assignment of long-lived dark states responsible for photoblinking to radicals was further supported by Zondervan and co-workers' study in which radical anions of rhodamine 6G (Rh6G), suggested to be formed via electron transfer from poly(vinyl alcohol) to Rh6G upon light irradiation, were observed in an electron-spin-resonance experiment.[20]

A new range of rhodamine-type molecules called Atto dyes has recently been demonstrated to be potential labels for use in fluorescent imaging.[21] In addition, the absence of cis−trans isomerization in these dyes enables one to neglect conformational changes as a source of photoblinking. We have chosen therefore to characterize the fluorescence intermittency and photobleaching kinetics of Atto565 (structure given in Chart 1) molecules immobilized on glass surface.

Due to the long triplet T_1 lifetime compared to the singlet S_1, the T_1 state has often been implicated in playing an active role in photoblinking and photobleaching processes.[11,12,22] To understand the importance of T_1 in affecting fluorescence intermittency, the T_1 state of Atto565 was first characterized using fluorescence correlation spectroscopy. Confocal microscopy was then used to investigate the photoblinking and photobleaching kinetics where power law kinetics for the photoblinking events are observed for Atto565.

There remains ambiguity concerning the pathways leading to the formation of the radical dark states.[16−20] It has often been proposed that charge transfer occurs *mainly* from the triplet T_1 state rather than from the singlet S_1 state.[20] However, detailed analysis of the possible pathways leading to the long-lived dark state of Atto565 in this work suggests the importance of charge transfer from the singlet S_1 state to the surrounding traps.

* Corresponding authors. E-mail: edwin.yeow@chem.kuleuven.be (E.K.L.Y.), johan.hofkens@chem.kuleuven.be (J.H.). Fax: (+32) 16327989.

10.1021/jp055496r CCC: $33.50
Published on Web 01/06/2006

CHART 1: Chemical Structure of Atto565

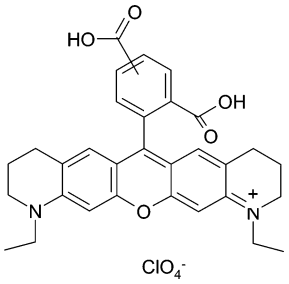

2. Experimental Section

In the fluorescence correlation spectroscopy (FCS) experiment, ca. 10^{-9} M aqueous solution of Atto565 (Atto-Tec) was excited at 543 nm using a continuous wave (cw) HeNe laser (Melles Griot). The excitation beam was directed into an inverted fluorescence microscope (Olympus IX 70), and focused onto the sample through an objective lens (Zeiss, 100x, N.A. 1.3, oil immersion). The fluorescence light was collected by the same objective and refocused through a pinhole (100 μm diameter). Unwanted scattered laser light was removed from the fluorescence signal using a notch filter, and the signal was then detected by an avalanche photodiode APD (SPCM 15, EG & G). The autocorrelation function was calculated from a digital correlator (ALV-5000, ALV GmbH).

The experimental setup used to record emission intensity time traces of single molecules dispersed onto glass surfaces is described in detail elsewhere.[23] Basically, an inverted microscope (Oympus IX 70) equipped with a scanning stage was used to detect single molecules. Time-resolved fluorescence decay curves were recorded by the time-correlated single photon counting technique (TCSPC) using a 543 nm pulsed laser light (8.18 MHz, 1.2 ps fwhm) excitation from a frequency doubled OPO (Spectra Physics) pumped by a mode-locked, regeneratively amplified Ti:Sapphire laser (Spectra Physics). The excitation light was focused through an oil immersion objective lens (Olympus, 100x, N.A. 1.4) which was also used to collect the fluorescence. A 50%/50% beam splitter divided the fluorescence signal into an APD for TCSPC measurements and into a CCD camera (LN/CCD-512SB, Princeton Instruments) coupled to a 150-mm polychromator (SpectraPro 150, Acton Research Coorp.) for fluorescence spectra measurements. Samples for single molecule experiments were prepared by spin-casting solutions of Atto565 in methanol ($\sim 10^{-10}$ M) onto thoroughly cleaned borosilicate glass coverslips (Menzel-Glaser).

The ensemble bleaching experiment was done by depositing a higher concentration of dye molecules (ca. 10^{-6} to 10^{-7} M) onto cleaned glass coverslips. At this concentration, aggregation and self-energy-transfer have been shown to be minimal.[24,25] The experimental setup is identical to the one for FCS and the sample was excited using a cw HeNe laser. Both single molecule and ensemble measurements were performed in air and nitrogen atmospheres. The latter was achieved by gently blowing nitrogen through the sample holder during the measurement.

3. Results and Discussion

3.1. Fluorescence Correlation Spectroscopy. Figure 1 shows the fluorescence autocorrelation curve obtained for Atto565 in aerated water using an excitation intensity (I) of 11 kW/cm^2. The autocorrelation curve was fitted to the function:[26]

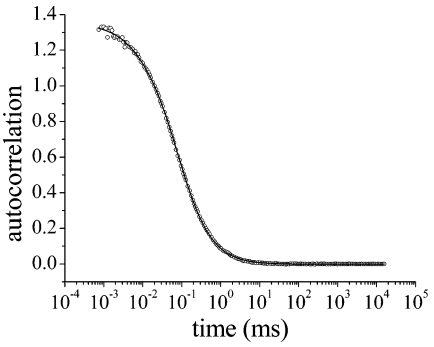

Figure 1. Autocorrelation curve for Atto565 in air atmosphere. Excitation wavelength was 543 nm.

$$G(t) = \frac{1}{N_{\text{eff}}}\left[\frac{1 - F + F\exp(-t/\tau_{\text{tri}})}{1 - F}\right] \times \left[\left(1 + \frac{t}{\tau_{\text{diff}}}\right)\left(1 + \frac{t}{\omega^2\tau_{\text{diff}}}\right)^{1/2}\right]^{-1} \quad (1)$$

where N_{eff} denotes the average number of molecules residing in the effective probe volume, F is the average fraction of molecules in the triplet state, ω describes the shape of the ellipsoidal detection volume ($\omega = z_o/r_o$, where z_o and r_o are the axial and lateral radii, respectively), and τ_{tri} and τ_{diff} are the triplet and diffusion relaxation time, respectively. The fitting analysis yielded values of 5.4×10^{-6} s and 0.0685 for τ_{tri} and F, respectively.

When a uniform excitation profile within the probe volume is assumed, τ_{tri} and F are given by[27]

$$\frac{1}{\tau_{\text{tri}}} = k_{\text{tri}} + \frac{k_{\text{ex}}k_{\text{isc}}}{k_s + k_{\text{ex}}} \quad (2)$$

$$F = \frac{k_{\text{ex}}k_{\text{isc}}}{k_{\text{ex}}(k_{\text{tri}} + k_{\text{isc}}) + k_s k_{\text{tri}}} \quad (3)$$

where k_s is the deexcitation rate from the excited singlet state (S_1) including fluorescence and internal conversion (2.94×10^8 s^{-1}), k_{isc} is the S_1-T_1 intersystem crossing rate, and k_{tri} is the decay rate from the triplet T_1 state. The excitation rate, k_{ex} ($=6.84 \times 10^6$ s^{-1}), was calculated from $k_{\text{ex}} = \sigma NI$, where σ is the absorption cross section of Atto565 at 543 nm (2.32×10^{-16} cm^2), and N is the number of photons in 1 J at 543 nm (2.73×10^{18} photons). From eqs 2 and 3, we obtained $k_{\text{isc}} = 5.58 \times 10^5$ s^{-1} and $k_{\text{tri}} = 1.73 \times 10^5$ s^{-1} for Atto565 in aerated water. These values are not significantly different from those determined for other rhodamine dyes such as rhodamine 6G (Rh6G) ($k_{\text{isc}} = 1.1 \times 10^6$ s^{-1} and $k_{\text{tri}} = 5.0 \times 10^5$ s^{-1} in water) and rhodamine 610 ($k_{\text{isc}} = 2.0 \times 10^5$ s^{-1} and $k_{\text{tri}} = 5.0 \times 10^5$ s^{-1} in ethylene glycol).[27,28]

3.2. Fluorescence Intensity Fluctuations. Typical emission intensity time traces of single Atto565 molecules on a glass surface under ambient conditions are shown in Figure 2. Figure 2a shows rapid emission intensity fluctuations with several long off periods. Similar photoblinking events with a duration lasting milliseconds to a few seconds are observed for other Atto565 molecules on the same glass surface. In Figure 2b, the molecule displays nearly constant emission intensity before undergoing irreversible photobleaching at around 105 s. Furthermore, a 330 ms off-time period is observed at about 28.8 s (see Figure 2c). Several explanations have been provided in the past to explain fluorescence intermittency, and the nature of long-lived dark

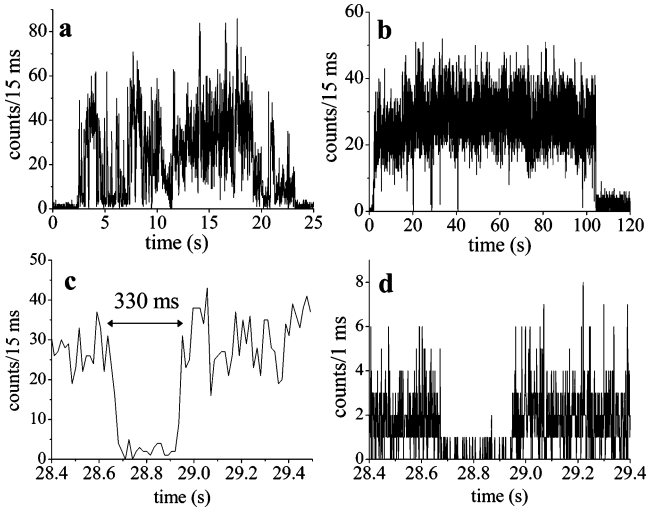

Figure 2. (a) Fluorescence intensity time trace of a single Atto565 molecule on glass surface with $I = 568$ W/cm^2 and in air atmosphere. (b) Fluorescence intensity time trace of another single Atto565 molecule on glass surface with $I = 568$ W/cm^2 and in air atmosphere. (c) Fluorescence intensity trace of (b) from 28.4 to 29.4 s magnified to show clearly an off-time of 330 ms at around 28.8 s. (d) The fluorescence intensity trace of (b) from 28.4 to 29.4 s with a smaller bin time of 1 ms.

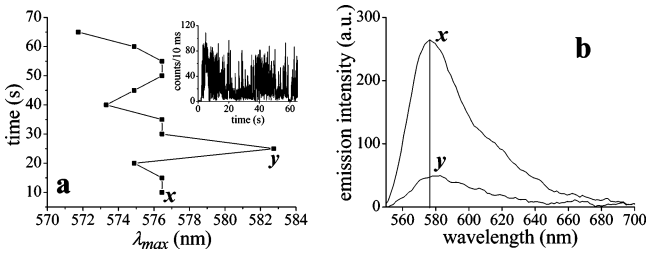

Figure 3. (a) Position of the maximum emission intensity wavelength (λ_{max}) vs time for the emission spectra recorded with 5 s integration time for the emission intensity time trace shown in the inset. (b) The emission spectra after 10 s (point *x* in Figure 3a) and 25 s (point *y* in Figure 3a).

states in dye molecules, namely, (1) intersystem crossing from an excited singlet state to a triplet (dark) state,[12] (2) rotation of the molecular dipole moment giving rise to variations in the amount of light absorbed and emitted,[11] and (3) spectral diffusion causing the absorption transition to shift in to and out of resonance with the excitation wavelength.[8,9,15]

Given that the triplet lifetime of Atto565 in air (i.e., ~6 μs) is much shorter than the observed long off-times discussed above, the triplet state is not responsible for photoblinking events occurring in this time regime (i.e., >1 ms). Furthermore, it has been demonstrated using fluorescence polarization experiments that rhodamine dye molecules tend to be rigidly immobilized on glass surfaces, thus hindering any molecular reorientation.[15,29] Rotational motion therefore plays an insignificant role in effecting fluorescence intensity fluctuations, especially because circular polarized light was used in all the single molecule measurements reported herein.

The influence of spectral diffusion is most pronounced at low temperature, where, due to the narrow absorption bandwidth, a small spectral shift results in a substantial change in the absorption cross section at the laser excitation frequency. This effect is drastically reduced at room temperature where a large shift in the broad absorption band is needed to account for changes in the emission intensity. Figure 3a shows the distribution of the maximum emission intensity wavelength (λ_{max}) as a function of time for a single Atto565 molecule (emission intensity time trace is given in the inset of Figure 3a). The emission spectra measured with 5 s integration time after 10 s (point *x* in Figure 3a) and 25 s (point *y* in Figure 3a) are displayed in Figure 3b. From Figure 3a, we note that λ_{max} varies between 571 and 583 nm. Assuming a Stokes shift of 870 cm^{-1} (from ensemble measurements), the absorption cross sections of the molecule at points *x* and *y* when excited at 543 nm differ by ca.. 1.2-fold which does not account for the ca. 5.3-fold reduction in the integrated fluorescence intensity (Figure 3b). Spectral diffusion is not, therefore, sufficient to describe completely the photoblinking events observed for Atto565 at room temperature, and other mechanisms must be sought to rationalize the long off-times.

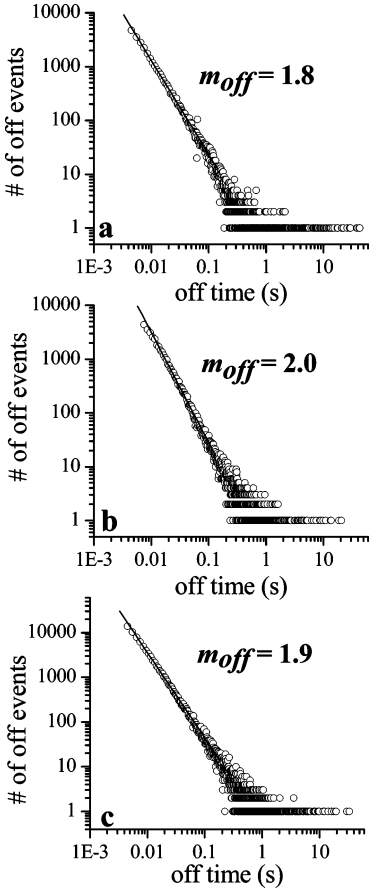

Figure 4. Off-time distributions for (a) 88 Atto565 molecules at 1136 W/cm^2, (b) 86 molecules at 568 W/cm^2, and (c) 73 molecules at 284 W/cm^2 in air atmosphere. The linear log−log plots indicate power law distribution, and the solid lines are lines of best fit with power law exponents $m_{off} = 1.8$ (a), 2.0 (b) and 1.9 (c).

3.3. On- and Off-Time Statistics. To characterize the fluorescence intermittency of Atto565 molecules, both on- and off-time duration histograms were constructed from emission time traces with 1 or 5 ms bin times. The number of counts associated with the observed detector background level after each molecule has undergone photobleaching is chosen to be the threshold value. The algorithm for creating on- and off- time histograms over large time range has been described in details elsewhere.[8,30,31] An insufficient number of on/off events per molecule renders the statistical analysis based on a single molecule unreliable, and the combined distribution of on/off events for 70−90 molecules is used instead. A small fraction of the molecules studied (<5%) did not display any long off-times of interest. Figure 4 shows the off-time duration histograms for 1 ms bin time obtained under ambient conditions for

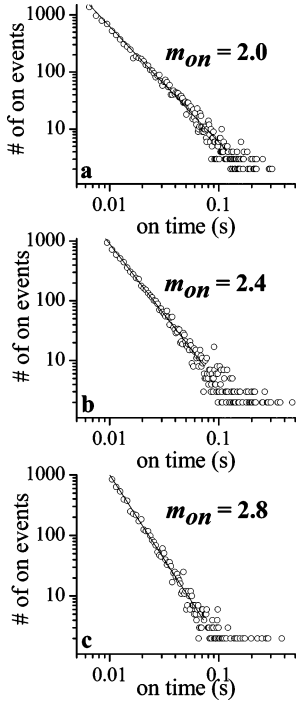

Figure 5. On-time distributions for (a) 88 Atto565 molecules at 1136 W/cm^2, (b) 86 molecules at 568 W/cm^2, and (c) 73 molecules at 284 W/cm^2 in air atmosphere. The linear log−log plots indicate power law distribution, and the solid lines are lines of best fit with power law exponents m_{on} = 2.0 (a), 2.4 (b) and 2.8 (c).

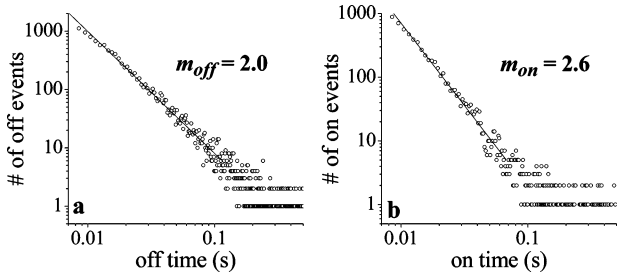

Figure 6. Off-time (a) and on-time (b) distributions for 74 Atto565 molecules at 568 W/cm^2 in N_2 atmosphere. The linear log−log plots indicate power law distribution, and the solid lines are lines of best fit with power law exponents m_{off} = 2.0 (a) and m_{on} = 2.6 (b).

excitation intensities (I) of 284, 568 and 1136 W/cm^2, and the corresponding on-time duration histograms are given in Figure 5. It is obvious from the linear log−log plots that the observed on/off-times cover a large time range and are described using a power law distribution:

$$P(\tau_{on/off}) = P_O \tau_{on/off}^{-m_{on/off}} \quad (4)$$

where $m_{on/off}$ is the power law exponent. The off-time distribution, $P(\tau_{off})$, is independent of excitation intensity with minimal changes in m_{off} ($\sim$1.9 within experimental error, $\pm$0.1). On the other hand, the on-time distribution, $P(\tau_{on})$, varies with excitation intensity such that reducing I increases m_{on}. The power law exponents do not change significantly when a larger bin time of 5 ms is used. In the case of I = 568 W/cm^2, m_{off} = 2.1 and m_{on} = 2.3. Similar photoblinking behavior is seen in nitrogen atmosphere, where linear double logarithmic plots for both on- and off-time duration histograms are obtained (see Figure 6 for I = 568 W/cm^2). The absence of an exponential distribution for τ_{off} indicates that in nitrogen the triplet lifetime is again too short to account for the long "off" events reported here.[12] The

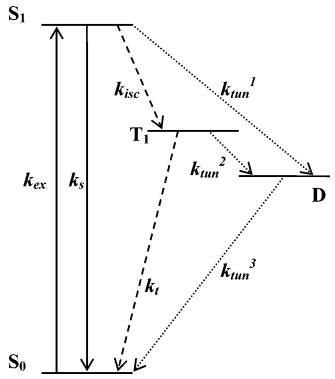

Figure 7. Four-level scheme used to describe the formation of the radical dark state D responsible for photoblinking events.

m_{off} (= 2.0 for I = 568 W/cm^2) and m_{on} (= 2.6 for I = 568 W/cm^2) values are in agreement with those obtained in air atmosphere, suggesting to a large extent oxygen-independent reactions as the source for the intermittency events. m_{off} values of 1.8−2.0 were also determined for Rh6G deposited on SiO_2 surfaces in various environments.[17]

The broad distribution of off-time durations can be explained using a charge tunneling model commonly employed to rationalize fluorescence intermittency in semiconductors,[30−32] and more recently in dye molecules.[16−20] In this case, a charge (most plausibly an electron) is transferred from Atto565 to localized states (i.e., charge traps) on the glass matrix. Subsequent charge recombination by back charge tunneling from the trap to the Atto565 cation restores the fluorescence. The radical dark state D is thus a radical pair consisting of the Atto565 cation and the ejected charge in the trap. The exponential distance dependence of the tunneling rate ensures power law statistics for the off-time durations, even when the distribution of the tunneling distance falls within a narrow range. The long-lived rhodamine 6G anion, suggested to be formed from electron transfer from poly(vinyl alcohol), PVA, to Rh6G, has previously been demonstrated to be the dark state responsible for photoblinking events in PVA film.[20] Electron transfer from dye molecules (e.g., rhodamine and perylene-3,4:9,10-tetracarboxylbisimide) to localized states on glass surfaces has also been reported.[25,33,34]

The construction of off-time distribution histograms by combining a number of molecules is commonly used to analyze fluorescence intermittency;[16−19] however, there may be disadvantages of doing so. In particular, as discussed by Hasse et al.[16] this method does not provide information on whether the distribution of rates is static or dynamic. However, power law kinetics for off events in a single molecule has been shown to agree with that for an ensemble of molecules.[18] The off-time exponent m_{off} is dependent on the tunneling barriers for both charge ejection and charge recombination.[32] Because the energy gap between the host matrix (e.g., glass, polymer film) and the dye molecules is large, the forward charge tunneling barrier for individual molecules remain relatively unchanged with respect to each other even though there is some fluctuation in the spectral mean for the different single molecules. Similarly, the tunneling barriers for charge recombination from traps (e.g., silica, PMMA) would be expected to be the same for the various single fluorescent systems (e.g, nanocrystal, terrylene) due to the large energy gap.[18,35] The off-time distributions obtained from either a single molecule or an ensemble of molecules should, therefore, provide similar information on the photoblinking kinetics.

On the basis of a simple four-level scheme (see Figure 7),

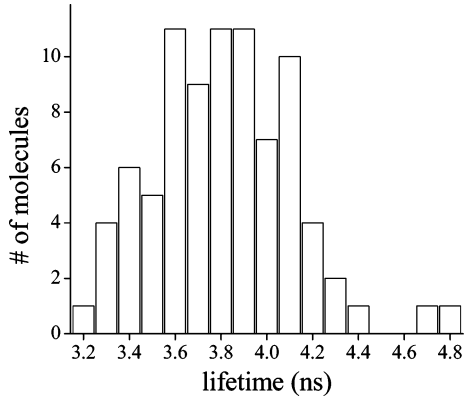

Figure 8. Distribution of single molecule fluorescence lifetime for 85 different Atto565 molecules using an excitation intensity of 568 W/cm^2 and in air atmosphere.

there exist two pathways leading to the formation of the dark state D. The first (route *a*) involves transition from S_1 to D via T_1, where charge transfer occurs from the intermediate triplet state, whereas the second (route *b*) entails direct charge tunneling from S_1 to charge traps to form D. Route *a* is often proposed to be the dominant pathway because of the greater probability for charge ejection to occur from the longer lived T_1 state (cf. S_1 state).[36] Unlike for route *b* where "off" to "on" transitions of interest occur solely from D and is therefore governed by the tunneling rate k^3_{tun} (see Figure 7), one needs, in the case of route *a*, to consider the combined decays from T_1 to D (and hence formation of D; k^2_{tun}) and subsequently from D to the "on" state (k^3_{tun}). For the latter case, m_{off} is governed by the process with the most spread out transition rate (i.e., k^2_{tun} or k^3_{tun}; see Appendix A).

We now consider the on-time distributions. Route *a* predicts an exponential distribution for on-time events, with average duration given by $\tau_{on} = (k_s + k_{isc})/(k_{isc}\ k_{ex})$,[12] which is inconsistent with the observed power law statistics. Deviation from exponential distribution could arise from fluctuations in the radiative and nonradiative decay rates. To study the significance of these effects, fluorescence lifetimes (τ_s) of single Atto565 molecules were obtained from their monoexponential emission decay profiles, and the τ_s distribution for $I = 568$ W/cm^2 is displayed in Figure 8. The lifetime distribution of single molecules dispersed on either glass surface or in polymer film has previously been attributed to an inhomogeneous matrix environment and electromagnetic boundary conditions.[37,38] In the case of Atto565, the emission lifetime ranges from 2.4 to 4.8 ns, with the majority of molecules (70%) experiencing a deexcitation rate (k_s) between 2.8×10^8 and 2.4×10^8 s^{-1}. The relatively small variation in k_s suggests that k_{isc} and k_t (which affect τ_{off} from T_1 in the absence of D) would need to span several orders of magnitude to achieve power law distributions for the photoblinking events. This requires extreme dynamic fluctuations in the environment (e.g., pressure, temperature and binding site properties) which are not present under the mild conditions used in our experiments.

Because triplet events such as $S_1 \rightarrow T_1$ intersystem crossing and $T_1 \rightarrow S_0$ relaxation are much shorter than the bin time used, on-time periods consisting of several unresolved triplet on/off events are separated by off-events (greater than bin time) arising from the charge separated state. From our Monte Carlo simulation study (discussed below), we note that the number of such on-time periods is too small to account for the large number of on-time events observed experimentally. In a typical computational experiment, where each emission intensity time trace lasts for 100 s, route *a* predicts a maximum of less than 5 on-time occurrences per bin for a sample size of 100 molecules. On the other hand, route *b* yields an exponential on-time distribution when charge tunneling to a static distribution of trap sites is assumed. Kuno et al. proposed a physical model based on slow fluctuation in the tunneling barrier height (ΔH) to at most a few traps to explain the on-time power law statistics observed in semiconductor quantum dots.[30,31] In this case, the effective tunneling rate, k^1_{tun}, is sensitive to changes in ΔH, and a small dynamic fluctuation in the environment (and hence ΔH) is sufficient to cause a large variation in k^1_{tun}.

Monte Carlo simulations were performed to test the validity of the two-pathway model. In the computational study, the tunneling rate constant k^i_{tun} (where $i = 1$, 2 or 3) is defined as[39]

$$k^i_{tun} = \kappa_i \exp(-x_i) \tag{5}$$

where the stochastic variable x_i is sampled from the normalized distribution $\Theta(x_i)$:

$$\Theta(x_i) = \gamma_i \exp(-\gamma_i x_i) \tag{6}$$

Equation 5 is the charge tunneling rate where the term x_i is defined by the tunneling length and tunneling barrier height. Equation 6 arises from the assumed exponential distribution of the fluctuating barrier (i.e., width and height).[39] For each iteration that describes the possible events occurring during one excitation deactivation cycle, random numbers are generated to determine the pathways taken for S_1 to go from "on" to "off" states (either route *a* or *b*), and for T_1 to decay (either to D or S_0). New x_i are then randomly selected to compute the necessary tunneling rates, whereas the other decay rates k_s, k_{isc} and k_t are fixed at 2.6×10^8, 10^5 and 10^5 s^{-1}, respectively. The tunneling rates k^1_{tun}, k^2_{tun}, and k^3_{tun} are independent of each other because the fluctuations in the different electronic levels of the molecule and its environment are different. The rates for all photophysical processes described by an exponential function (i.e., k_s, k_{isc} and k_t) are based on values close to the experimental values obtained from either fluorescence correlation spectroscopy (section 3.1) or single molecule fluorescence lifetime measurements. The simulation in Figure 9a shows the first 50 s (of the 100 s) of the emission intensity time trace for a single molecule with $\kappa_1 = 4 \times 10^9$ s^{-1}, $\kappa_2 = \kappa_3 = 10^6$ s^{-1}, and $\gamma_i = 1$ for $i = 1$, 2 and 3. The proper choice of κ_i is necessary to adequately describe the power-law behavior in any given experimental time window.[39] A background of 1000 counts/s was included to mimic actual experimental conditions, and bin times of 1 ms and $k_{ex} = 4.1 \times 10^5$ s^{-1} were chosen. Parts b and c of Figure 9 display the off- and on-time duration histograms, respectively, for a collection of 100 molecules when a threshold value of 6 counts/bin is used. The threshold values were chosen to be slightly higher ($2-3\sigma$) than the background noise level. Linear log−log plots with gradients $m_{off} = 2.0$ and $m_{on} = 2.6$ are obtained. Increasing the threshold to 8 counts/bin did not alter the value of m_{off}, and only slightly reduced m_{on} to 2.5. When route *a* is the only pathway to form D, power law statistics for "on" events are never observed in the simulations. This demonstrates that both routes *a* and *b* are needed to properly reproduce the fluorescence intermittency behavior observed experimentally. It is worth noting that route *b* alone describes a power law behavior; however, there is no experimental evidence to exclude route *a*. Because route *a* involves the relatively longer lived T_1 state, it is likely that this pathway is also involved in the formation of the radical state.

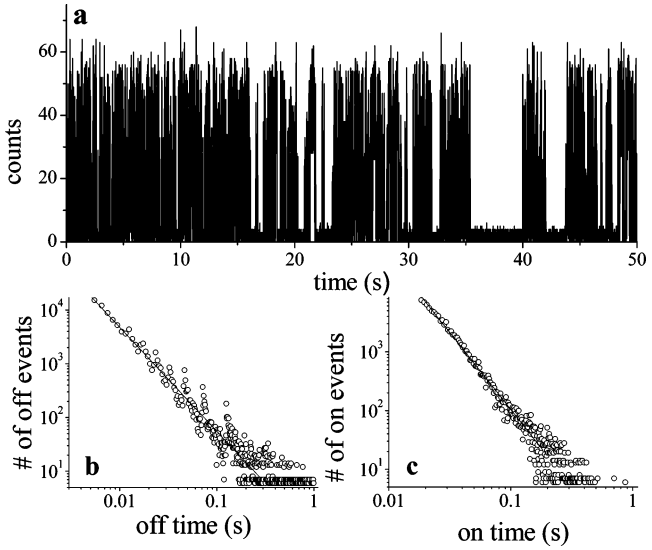

Figure 9. (a) Monte Carlo simulations of the fluorescence intensity time trace based on the four-level scheme. Only half of the trajectory (bin time = 1 ms) is presented. Both off-time (b) and on-time (c) distributions yield straight lines on log−log plots. The solid lines are linear fits to the data.

To understand the dependence of the power law exponent m_{on} on excitation intensity, various k_{ex} (e.g., 2.5×10^5 and 5.7×10^5 s^{-1}) were used in the Monte Carlo simulations. Although m_{off} remains basically unchanged, m_{on} increases with excitation intensities such that $m_{on} = 2.4$, 2.6 and 2.8 for $k_{ex} = 2.5 \times 10^5$, 4.1×10^5 and 5.7×10^5 s^{-1}, respectively. This arises from the greater number of excitation cycles in a given unit of time (i.e., excited-state population) at high excitation intensity, which leads to a less spread out on-time duration. Unfortunately, this does not concur with the inverse relationship seen between experimental m_{on} and I. A plausible explanation for this is the involvement of photoinduced processes in changing the molecular environment whereby high excitation intensities lead to stronger interactions between the molecule and its surrounding phonons. The molecule thus accesses different potential minima, which results in a dynamic, albeit small, alteration of ΔH and a wide range of values for k^1_{tun}. The inverse relationship between m_{on} and I can now be understood using this simple model. At high excitation rate, there is a greater chance for the molecule to be in a vastly different energy minimum between adjacent "on" events, thus resulting in a more significant change in ΔH, and a larger spread in k^1_{tun} (i.e., smaller m_{on}). The lack of excitation intensity dependence of m_{off} suggests that charge trap sites are impervious to light induced processes. It must be stressed, however, that this mechanism is not rigorously proven here, and further systematic experiments must be conducted to gain better insight into the relationship between m_{on} and I.

3.4. Single Molecule and Ensemble Photobleaching. The survival (or bleaching) time histograms of single Atto565 molecules in ambient conditions are displayed in Figure 10 for various excitation intensities (i.e., 1136, 568 and 284 W/cm^2). For comparison purposes, block widths of 10 s were used to construct the histograms. It is clear that the bleaching times do not decay monoexponentially, especially at low excitation intensities. In particular, a few long surviving molecules can be seen contributing to the nonexponential tail at long times. Nonetheless, approximate average bleaching times (τ_{bl}) of 18.2, 21.8 and 63.0 s were obtained for $I = 1136$, 568 and 284 W/cm^2, respectively, by fitting the histograms with a single-exponential function. As expected, Atto565 molecules undergo faster photobleaching at higher excitation intensities.

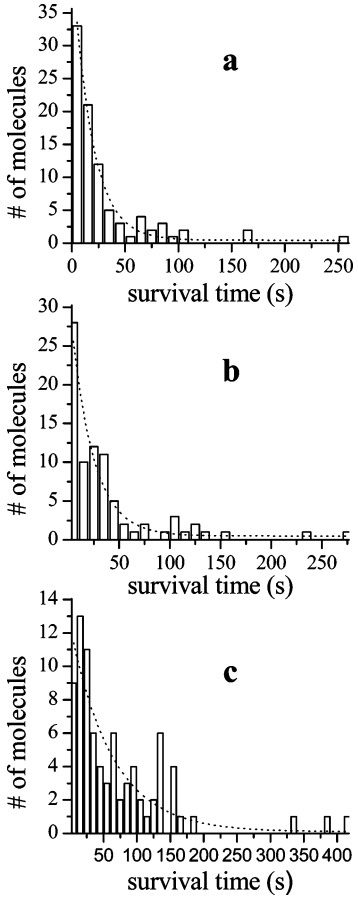

Figure 10. Bleaching time histograms for (a) 90 Atto565 molecules at 1136 W/cm^2, (b) 82 molecules at 568 W/cm^2, and (c) 81 molecules at 284 W/cm^2 in air atmosphere. The dotted curves are monoexponential fits to the histograms, yielding approximate average bleaching times of 18.2 (a), 21.8 (b), and 63.0 s (c).

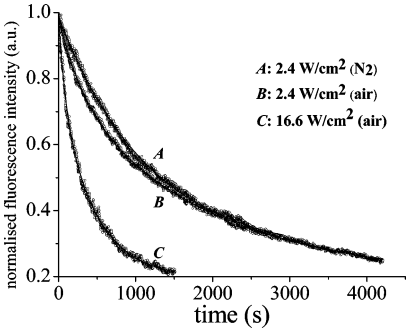

Figure 11. Decay of the fluorescence intensity of an ensemble of Atto565 molecules under excitation intensity of 2.4 W/cm^2 in N_2 (A) and air (B), and at a higher excitation intensity of 16.6 W/cm^2 in air (C). The bleaching curves in N_2 and air were fitted to monoexponential and biexponential functions, respectively (shown solid curves).

The bleaching curves for an ensemble of Atto565 molecules deposited on a glass surface are given in Figure 11 for two excitation intensities $I = 2.5$ and 16.5 W/cm^2. The fluorescence intensity measured in nitrogen atmosphere at $I = 2.5$ W/cm^2 decays monoexponentially with a rate of 8.5×10^{-4} s^{-1} ($\tau_{bl} =$ 19.6 min). On the other hand, in air atmosphere and at the same I, the fluorescence intensity exhibits a biexponential decay with rates $k_1 = 5.1 \times 10^{-4}$ s^{-1} ($\tau_{bl} = 32.6$ min) and $k_2 = 2.9 \times 10^{-3}$ s^{-1} ($\tau_{bl} = 5.7$ min). Upon increasing I to 16.6 W/cm^2, the bleaching curve in air atmosphere continues to display a biexponential decay but with faster rates of $k_1 = 2.2 \times 10^{-3}$

s^{-1} ($\tau_{bl} = 7.7$ min) and $k_2 = 1.2 \times 10^{-2}$ s^{-1} ($\tau_{bl} = 83.2$ s), in agreement with the trend observed in the single molecule experiment.

Biexponential fits to the experimental bleaching curves in air atmosphere can be rationalized in terms of two subpopulations of the molecules (i.e., population 1 and population 2).[20,36,40] Molecules of population 1 do not form any dark radical D states, and the bleached state B is formed directly from the triplet T_1 state. The second bleaching rate constant arises from population 2 where molecules in this subpopulation form the radical D state from routes *a* and *b*. The effective bleaching rate constant is dependent on both the bleaching rates from T_1 to B, and from D to B. The quenching mechanism is most likely due to an oxygen-dependent reaction whereby reactive singlet oxygen ($^1O_2$) formed from the reaction between T_1 and triplet oxygen ($^3O_2$) can attack and eventually destroy the molecules. The radical state can also react with oxygen to form photooxidized bleached products. Because the lifetime of D is longer than T_1, we attribute k_1 to population 2 and k_2 to population 1. Analytical expressions based on the steady-state approximation for the bleaching rate constants for both subpopulations are given in Appendix B. In the absence of oxygen, only a monoexponential bleaching decay is observed. This is probably due to the bleaching of molecules belonging to population 1, whereas the bleaching time of population 2 molecules is too long to be recorded in our experimental time window. Two possible bleaching mechanisms might be (1) if the sample is not fully deoxygenated, there remain minute amounts of $^3O_2$ that can react with T_1 or D, and (2) oxygen-independent bleaching mechanisms such as reactions between T_1/D and the surrounding matrix to form the bleached products.

4. Conclusion and Final Remarks

We have studied the photoblinking of single Atto565 molecules dispersed on glass surface in air and nitrogen atmospheres. The broad time duration distributions for both on- and off-events follow power law statistics and is attributed to a long-lived dark state comprising an Atto565 cation and a trapped charge. Two primary pathways have been identified to be responsible for the formation of the radical dark state: (1) direct tunneling from the excited singlet S_1 state to charge traps and (2) an indirect route involving intersystem crossing from S_1 to the triplet T_1 state, followed by charge transfer from T_1. Monte Carlo simulations were able to reproduce the fluorescence intermittency kinetics based on the two-pathway model. In addition, the off-exponent m_{off} is insensitive to changes in excitation intensity, whereas the on-exponent m_{on} exhibits an inverse relationship with *I*. Nonexponential photobleaching kinetics observed for single and ensemble molecules in air atmosphere suggest the existence of multiple pathways leading to the formation of the bleached product. Apart from the triplet state, radical dark states can react with oxygen to form active oxygen or photooxidized bleached products that irreversibly destroy the molecule.

As discussed in the Introduction, blinking poses a serious problem for studies requiring fluorescent probes to emit light with minimal interruptions. Long on/off events can be suppressed by either eliminating the formation of the radical dark state, or by promoting rapid charge recombination back to the light emitting neutral state. The addition of chemical stabilizers (e.g., reducing or oxidizing agents) may help to reduce unwanted photoblinking occurrences.[41] Furthermore, they are known to impede the photobleaching rates of some organic molecules as well.[42]

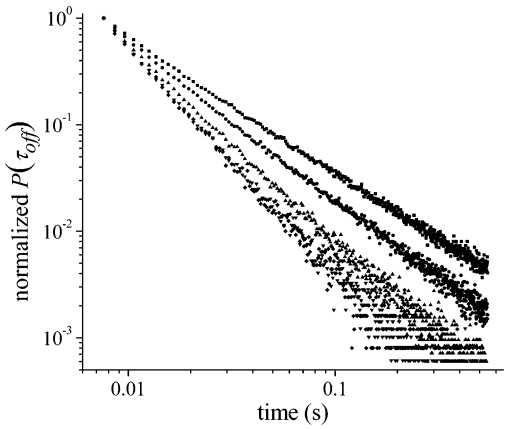

Figure A1. Normalized off-time distribution $P(\tau_{off})$ based on the Monte Carlo modeling of the convolution of the transit times from T_1 to D, and from D to S_0 for $\beta = 1$ and $\alpha = 0.2$ (■), 0.4 (●), 0.7 (▲), 2 (▼), and 1 (♦).

TABLE A1: Simulated off-time Exponent m_{off} for Different Combinations of α and β[a]

α (1 + α′)[b]	β (1 + β′)[c]	m_{off}
0.2 (1.24)	1 (2.09)	1.28
0.4 (1.46)	1 (2.07)	1.52
0.7 (1.79)	1 (2.12)	1.86
2 (3.18)	1 (2.07)	2.09
1 (2.12)	1 (2.13)	2.12
1 (2.13)	0.7 (1.79)	1.87
1 (2.12)	0.4 (1.46)	1.52
1 (2.11)	0.2 (1.25)	1.29

[a] The transit times are generated from a power law distribution $ip^i\tau^{-(1+i)}$ for $i = \alpha$ or β, and $p = 10^{-4}$. [b] $(1 + \alpha')$ refers to the power law exponent for the distribution of the transit time from T_1 to D obtained from the Monte Carlo simulations. [c] $(1 + \beta')$ refers to the power law exponent for the distribution of the transit time from D to S_0 obtained from the Monte Carlo simulations.

The fluorescence intermittency behavior arising from intermolecular electron transfer between dye molecules and electron traps found in the surrounding matrix is different from that resulting from intramolecular electron-transfer processes occurring within single donor−acceptor based systems. Long off-times observed in the latter are due mainly to cycles of rapid charge separation followed by charge recombination to the ground state,[3,14] whereas single cycles of these events are responsible for off-events seen in the former. Changes in the properties of fluorescence intermittency with respect to electron-transfer mechanism (e.g., electron tunneling versus conventional Marcus-type[43]) will be addressed in a forthcoming paper.

Appendix A

We have assumed that the charge recombination (tunneling) rate from the trapped charge to the cationic Atto565 is k_{tun}^3 regardless of the path taken. If the probability distributions of the transition times from T_1 to D and from D to S_0 are $P_2(\tau) = \alpha p^\alpha \tau^{-(1+\alpha)}$ and $P_3(\tau) = \beta p^\beta \tau^{-(1+\beta)}$, respectively, then the overall off-time distribution for route *a* is given by the convolution of $P_2(\tau)$ and $P_3(\tau)$. Monte Carlo simulations were employed to model the convolution, whereby the set of times $\{\tau_i\}$ distributed according to $P_{2(or3)}(\tau)$ was generated via $\tau_i = p(1 - r_j)^{-1/\alpha(or\ \beta)}$, and $\{r_j\}$ is a set of uniformly distributed numbers in the interval [0, 1]. The distribution of τ_{off} is displayed in Figure A1 for $\beta = 1$ and various α values, and Table A1 gives the off-time power exponent, m_{off}, obtained from the Monte Carlo simulations for different combinations of α and β. Clearly, m_{off} has a numerical

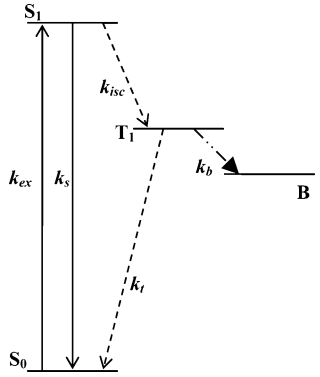

Figure A2. Energy level diagram for molecules undergoing bleaching from triplet T_1 state. B is the bleached state.

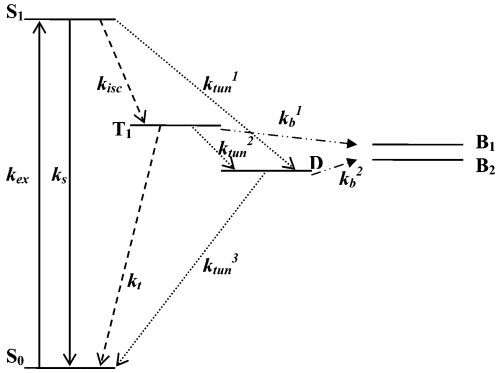

Figure A3. Energy level diagram for molecules undergoing bleaching from both triplet T_1 and radical D states. The bleached states formed from T_1 and D are B_1 and B_2, respectively, which may or may not be similar bleached products.

value of ξ when α and β are either equal or close to $(\xi - 1)$. Furthermore, m_{off} is skewed toward the tunneling process with the most spread out transition rate (i.e., k^2_{tun} or k^3_{tun}). For an example, for m_{off} to take on a value of ξ for $\beta = (\xi - 1)$, k^2_{tun} should be significantly faster than k^3_{tun} (e.g., $\alpha = 2$ and $\beta = 1$ for $m_{off} = 2.09$ in Table A1). Indeed, when the charge's potential in the trap is lower than its potential in the triplet state (relative to the glass matrix), a faster forward T_1 to D transition is expected as a result of a smaller charge tunneling barrier height. This corresponds to Zondervan and co-workers' observation of very rapid population of D from T_1 as compared to the intersystem crossing rate for Rh6G.[20,36]

Appendix B

For population *1*, the time-resolved probability that a molecule is in state *i* (i.e., S_0, S_1 or T_1) is obtained by solving the following set of kinetic equations (see Figure B1):

$$dS_0/dt = -k_{ex}S_0 + k_sS_1 + k_tT_1$$
$$dS_1/dt = k_{ex}S_0 - (k_s + k_{isc})S_1$$
$$dT_1/dt = k_{isc}S_1 - (k_t + k_b)T_1$$

By assuming that the photobleaching rate constant k_b is much smaller than all other rate constants, we solve the above set of equations using the steady-state approximation (i.e., $dS_0/dt = dS_1/dt = dT_1/dt = 0$, and $S_0 + S_1 + T_1 = 1$). In this way, S_0, S_1 and T_1 are expressed as follows:

$$S_0 = 1 + \frac{k_t(k_s + k_i)}{k_{ex}(k_t + k_i)}$$
$$S_1 = \frac{k_{ex}S_0}{k_s + k_{isc}}$$
$$T_1 = \frac{k_{isc}S_1}{k_t + k_b}$$

The bleaching process is described by the monoexponential function $D(t) = D_0 \exp[-(k_bT_1)t]$, and the survival time is given by $1/(k_bT_1)$. In the case of population 2, the probability that a molecule is in a particular state *i* (i.e., S_0, S_1, T_1 or D) is obtained by solving the following set of equations (see Figure B2),

$$dS_0/dt = -k_{ex}S_0 + k_sS_1 + k_tT_1 + k_{tun}{}^3D$$
$$dS_1/dt = k_{ex}S_0 - (k_s + k_{isc} + k^1_{tun})S_1$$
$$dT_1/dt = k_{isc}S_1 - (k_t + k^2_{tun} + k^1_b)T_1$$
$$dD/dt = k^2_{tun}T_1 - (k^3_{tun} + k^2_b)D$$

From steady-state approximation, the solutions are

$$S_0 = A/B$$
$$S_1 = \frac{k_{ex}S_0}{k_s + k_{isc} + k^1_{tun}}$$
$$T_1 = \frac{k_{isc}S_1}{k_t + k^2_{tun} + k^1_b}$$
$$D = \frac{k^2_{tun}T_1}{k^3_{tun} + k^2_b}$$

where

$$A = -(-k_{isc}k_tk^3_{tun} - k_{isc}k_tk^2_b - k^1_{tun}k_tk^3_{tun} - k^1_{tun}k_tk^2_b + k^2_{tun}k_sk_tT_1 + k^2_{tun}k_{isc}k_tT_1 + k^2_{tun}k^1_{tun}k_tT_1 - k_sk_tk^3_{tun} - k_sk_tk^2_b - k^3_{tun}k^2_{tun}k_sT_1 - k^3_{tun}k^2_{tun}k_{isc}T_1 - k^3_{tun}k^2_{tun}k^1_{tun}T_1)$$

and

$$B = k_sk_tk^2_b + k_{isc}k_tk^3_{tun} + k_{isc}k_tk^2_b + k_sk_tk^3_{tun} + k_{ex}k_tk^2_b + k^1_{tun}k_tk^3_{tun} + k^1_{tun}k_tk^2_b + k_{ex}k_tk^3_{tun} + k_{ex}k^1_{tun}k^3_{tun} + k_{ex}k^1_{tun}k^2_b + k_{ex}k_{isc}k^3_{tun} + k_{ex}k_{isc}k^2_b$$

The bleaching process is also described by the monoexponential function $D'(t) = D_0' \exp[-(k^1_bT_1 + k^2_bD)t]$, where the survival time of the molecules is $1/(k^1_bT_1 + k^2_bD)$.

Acknowledgment. Support from the FWO, the Flemish Ministry of Education (GOA 2001/2002) and the BMBF, the Federal Science Policy of Belgium (IAP-V-03) is acknowledged. A Max Planck research award and a Eurocores grant (Bionics) are also acknowledged.

References and Notes

(1) Schuler, B. *ChemPhysChem* **2005**, *6*, 1206.
(2) Velonia, K.; Flomenbom, O.; Loos, D.; Masuo, S.; Cotlet, M.; Engelborghs, Y.; Hofkens, J.; Rowen, A. E.; Klafter, J.; Nolte, R. J. M.; De Schryver, F. C. *Angew. Chem., Int. Ed.* **2004**, *43*, 2.
(3) Bell, T. D. M.; Stefan, A.; Masuo, S.; Vosch, T.; Lor, M.; Cotlet, M.; Hofkens, J.; Bernhardt, S.; Müllen, K.; Van der Auweraer, M.; Verhoeven, J.; De Schryver, F. C. *ChemPhysChem* **2005**, *6*, 942.
(4) Eggeling, C.; Volkmer, A.; Seidel, C.A. M. *ChemPhysChem* **2005**, *6*, 791.
(5) Windergren, J.; Rigler, R. *Bioimaging* **1996**, *4*, 149.
(6) Füreder-Kitzmüller, E.; Hesse, J.; Ebner, A.; Gruber, H. J.; Schütz, G. J. *Chem. Phys. Lett.* **2005**, *404*, 13.
(7) Gensch, T.; Böhmer, M.; Aramendía, P. F. *J. Phys. Chem. A* **2005**, *109*, 6652.
(8) Weston, K. D.; Carson, P. J.; Metiu, H.; Buratto, S. K. *J. Chem. Phys.* **1998**, *109*, 7474.
(9) Weston, K. D.; Buratto, S. K. *J. Phys. Chem. A* **1998**, *102*, 3635.
(10) Ha, T.; Enderle, Th.; Chemla, D. S.; Selvin, P. R.; Weiss, S. *Chem. Phys. Lett.* **1997**, *271*, 1.
(11) Ambrose, W. P.; Goodwin, P. M.; Martin, J. C.; Keller, R. A. *Phys. Rev. Lett.* **1994**, *72*, 160.
(12) Yip, W.-T.; Hu, D.; Yu, J.; Vanden Bout, D. A.; Barbara, P. F. *J. Phys. Chem. A* **1998**, *102*, 7564.
(13) Köhn, F.; Hofkens, J.; Gronheid, R.; Van der Auweraer, M.; De Schryver, F. C. *J. Phys. Chem. A* **2002**, *106*, 4808.
(14) Cotlet, M.; Masuo, S.; Luo, G. B.; Hofkens, J.; Van der Auweraer, M.; Verhoeven, J.; Müllen, K.; Xie, X. S.; De Schryver, F. C. *P. Natl. Acad. Sci. U.S.A.* **2004**, *101*, 14343.
(15) Lu, H. P.; Xie, X. S. *Nature* **1997**, *385*, 143.
(16) Haase, M.; Hübner, C. G.; Reuther, E.; Herrmann, A.; Müllen, K.; Basché, Th. *J. Phys. Chem. A* **2004**, *108*, 10445.
(17) Schuster, J.; Cichos, F.; von Borczyskowski, C. *Opt. Spectrosc.* **2005**, *98*, 778.
(18) Schuster, J.; Cichos, F.; von Borczyskowski, C. *Appl. Phys. Lett.* **2005**, *87*, 051915.
(19) Hoogenboom, J. P.; van Dijk, E. M. H. P.; Hernando, J.; van Hulst, N. F.; García-Parajó M. F. *Phys. Rev. Lett.* **2005**, *95*, 097401.
(20) Zondervan, R.; Kulzer, F.; Orlinskii, S. B.; Orrit, M. *J. Phys. Chem. A* **2003**, *107*, 6770.
(21) Marmé, N.; Knemeyer, J.-P.; Sauer, M.; Wolfrum, J. *Bioconjugate Chem.* **2003**, *14*, 1133.
(22) Eggeling. C.; Widengren, J.; Rigler, R.; Seidel, C. A. M. *Anal. Chem.* **1998**, *70*, 2651.
(23) Vosch, T.; Cotlet, M.; Hofkens, J.; Van Der Biest, K.; Lor, M.; Weston, K.; Tinnefeld, P.; Sauer, M.; Latterini, L.; Müllen, K.; De Schryver, F. C. *J. Phys. Chem. A* **2003**, *107*, 6920.
(24) Köhn, F.; Hofkens, J.; De Schryver, F. C. *Chem. Phys. Lett.* **2000**, *321*, 372.
(25) Liang, Y.; Ponte Goncalves, A. M. *J. Phys. Chem.* **1985**, *89*, 3290.
(26) Krichevsky, O.; Bonnet, G. *Rep. Prog. Phys.* **2002**, *65*, 251.
(27) Windergren, J.; Mets, Ü.; Rigler, R. *J. Phys. Chem.* **1995**, *99*, 13368.
(28) Menzel, R.; Thiel, E. *Chem. Phys. Lett.* **1998**, *291*, 237.
(29) Weber, M. A.; Stracke, F.; Meixner, A. J. *Cytometry* **1999**, *36*, 217.
(30) Kuno, M.; Fromm, D. P.; Hamann, H. F.; Gallagher, A.; Nesbitt, D. J. *J. Chem. Phys.* **2000**, *112*, 3117.
(31) Kuno, M.; Fromm, D. P.; Hamann, H. F.; Gallagher, A.; Nesbitt, D. J. *J. Chem. Phys.* **2001**, *115*, 1028.
(32) Verberk, R.; van Oijen, A. M.; Orrit, M. *Phys. Rev. B* **2002**, *66*, 233202.
(33) Lee, M.; Kim, J.; Tang, J.; Hochstrasser, R. M. *Chem. Phys. Lett.* **2002**, *359*, 412.
(34) Zang, L.; Liu, R.; Holman, M. W.; Nguyen, K. T.; Adams, D. M. *J. Am. Chem. Soc.* **2002**, *124*, 10640.
(35) Verberk, R.; Chon, J. W. M.; Gu, M.; Orrit, M. *Physica E* **2005**, *26*, 19.
(36) Zondervan, R.; Kulzer, F.; Kol'chenko, M. A.; Orrit, M. *J. Phys. Chem. A* **2004**, *108*, 1657.
(37) Xie, X. S. *Acc. Chem. Res.* **1996**, *29*, 598.
(38) Vallée, R.; Tomczak, N.; Gersen, H.; van Dijk, E. M. H. P.; García-Parajó, M. F.; Vancso, G. J.; van Hulst, N. F. *Chem. Phys. Lett.* **2001**, *348*, 161.
(39) Kuno, M.; Fromm, D. P.; Johnson, S. T.; Gallagher, A.; Nesbitt, D. J. *Phys. Rev. B* **2003**, *67*, 125304.
(40) Molski, A. *J. Chem. Phys.* **2001**, *114*, 1142.
(41) Hohng, S.; Ha, T. *J. Am. Chem. Soc.* **2004**, *126*, 1324.
(42) Dittrich, P. S.; Schwille, P. *Appl. Phys. B* **2001**, *73*, 829.
(43) Leite, V. B. P.; Alonso, L. C. P.; Newton, M.; Wang, J. *Phys. Rev. Lett.* **2005**, *95*, 118301.